



# An In-Depth Optimization of Thickness of Base and Emitter of ZnO/Si Heterojunction-Based Crystalline Silicon Solar Cell: A Simulation Method

Houcine Naim<sup>1,2</sup> · Deb Kumar Shah<sup>3,4</sup> · Abed Bouadi<sup>1,2</sup> · Masoom Raza Siddiqui<sup>5</sup> · M. Shaheer Akhtar<sup>4,6</sup> · Chong Yeal Kim<sup>6</sup>

Received: 15 September 2021 / Accepted: 8 November 2021 / Published online: 1 December 2021

© The Minerals, Metals & Materials Society 2021

## Abstract

The heterojunction (HJ) solar cell is one of the best possible options to upgrade the conventional single homo-junction c-Si solar cell. In this work, a single HJ solar cell based on crystalline silicon (c-Si) wafer with zinc oxide (ZnO) is designed to reduce the loss of power conversion owing to the reflection of incident photons by the top surface of silicon. A PC1D simulation is used to evaluate the optimum numerical value of key photovoltaic parameters for HJ-based c-Si solar cells. The average reflectance for ZnO/Si HJ-based c-Si is 7.65% in the wavelength range of 400–1000 nm. The highest efficiency ( $\eta = 24.8\%$ ) of the ZnO/Si HJ-based c-Si solar is obtained with a 400  $\mu\text{m}$  base thickness, 20  $\mu\text{m}$  emitter thickness, doping concentration of  $1.1 \times 10^{17} \text{ cm}^{-3}$  in the base and a doping concentration of  $5.1 \times 10^{16} \text{ cm}^{-3}$  in the emitter. The proposed ZnO/Si HJ-based c-Si solar cell with high efficiency would be one of the best possible alternative HJ device to the conventional single homo-junction c-Si solar cell.

**Keywords** Silicon solar cell · zinc oxide · heterojunction · thickness · emitter · base · PC1D · simulation

---

Houcine Naim and Deb Kumar Shah equally contributed to this work

✉ M. Shaheer Akhtar  
shaheerakhtar@jbnu.ac.kr

✉ Chong Yeal Kim  
kimbo@jbnu.ac.kr

<sup>1</sup> Laboratory Industrial Engineering and Sustainable Development, University Center Relizane, 48000 Relizane, Algeria

<sup>2</sup> Laboratory for Analysis and Applications of Radiation (LAAR), Department of Physics, University of Science and Technology of Oran (USTO), 31024 Oran, Algeria

<sup>3</sup> School of Semiconductor and Chemical Engineering, Jeonbuk National University, Jeonju 54896, Republic of Korea

<sup>4</sup> Graduate School of Integrated Energy-AI, Jeonbuk National University, Jeonju 54896, Republic of Korea

<sup>5</sup> Chemistry Department, College of Science, King Saud University, Riyadh 11451, Saudi Arabia

<sup>6</sup> New and Renewable Energy Materials Development Center (NewREC), Jeonbuk National University, Jeonbuk 56332, Republic of Korea

## Introduction

Semiconductors, especially transparent conductive oxides (TCO), exhibit the larger energy bandgap ( $>3.0 \text{ eV}$ ), direct current resistivity (n-type) up to  $10^{-5}$ – $10^{-4} \Omega \text{ cm}$ , and good transmittance ( $>80\%$ ) in the visible range, which are commonly used as front electrodes in almost all thin-film solar cells.<sup>1–5</sup> Binary and ternary oxide systems such as  $\text{SnO}_2$ ,  $\text{CdO}$ ,  $\text{In}_2\text{O}_3$ ,  $\text{ZnO}$ ,  $\text{Ga}_2\text{O}_3$ ,  $\text{Cu}_2\text{O}$ ,  $\text{SrTiO}_3$ , and their different doping systems, are the common TCO thin films. When elements (Sn, In, Zn, and Cd) react with oxygen, their d-electron orbitals are filled, which is a basic characteristic of the binary oxide system.<sup>6,7</sup> A highly transparent TCO with less conductivity can be applied at the front side resulting in a higher current density. Furthermore, the hole contact formation in the heterojunction (HJ) is often considered to be more delicate compared to the electron contact.<sup>8</sup> Zinc oxide (ZnO) is a promising TCO material in the photovoltaic industry due to its abundance, relatively low deposition temperature, low production cost, simple processing steps, and low toxicity.<sup>9–12</sup> However, n-ZnO has been discovered to have applications in a variety of optoelectronic devices, including photovoltaic cells. Several researchers have used

n-ZnO thin films to fabricate possibly high-efficiency, low-cost solar cells, since the use of n-ZnO as an emitter layer and antireflection (AR) coating layer has been proposed.<sup>13,14</sup> Considering the importance of the optical properties of ZnO as a front n-layer, the front ZnO film is intended to act as antireflection coating as well as an electrically active layer in p-n junction formation. The advantages of hetero p-n junction solar cells are the liberty to choose a material, layer thickness, dopant concentrations, inherent surface passivation, and low-temperature approach.<sup>15</sup> As a result, ZnO/Si HJ-based solar cells may be more competitive technology in the future photovoltaic market. Other metal-oxides-derived single Si HJ-based solar cells have also been demonstrated by various researchers. Gerling et al. manufactured single heterojunction (SHJ)-based solar cells by depositing thermally evaporated transition metal oxides as front p-type contacts in planar n-type c-Si solar cells. Among different transition metal oxides, the highest power conversion efficiency of 12.7% with a  $V_{oc}$  value of 593 mV was reported for  $V_2O_5$ , as compared to other  $MoO_3$  and  $WO_3$  as the p-layer.<sup>16</sup> Recently, NiOx/Si HJ-based solar cells have been fabricated with nickel oxide ( $NiO_x$ ) as a p-selective layer and n-type Si as an active absorption layer and reported a promising efficiency of 12.73% as the  $V_{oc}$  increased from 423 to 906.16 mV with an  $NiO_x$  layer in SHJ solar cells.<sup>17</sup>

HJ-based c-Si solar cells have recently gained a great deal of attention because they present reasonably high power conversion efficiency (PCE) up to 24.7%,<sup>18–20</sup> relatively low fabrication temperature,<sup>21</sup> low fabrication cost, and low-temperature dependence on conversion efficiency.<sup>22</sup> The HJ cells use a c-Si wafer as an emitter with a huge bandgap of hydrogenated amorphous silicon (a-Si:H), and the charge carriers can only travel in one direction due to the greater band offset.<sup>23</sup> In single HJ c-Si solar cell, the recombination time would primarily affect  $V_{oc}$ , loss in resistance which affect fill factor (FF), and the optical losses affect directly  $I_{sc}$ .<sup>24</sup>

Chen et al. deposited ZnO:B (B-doped ZnO) thin films by the metal organic chemical vapor deposition (MOCVD) method and performed a computational study of n-ZnO/p-Si HJ-based solar cells using AFORS-HET tools. n-ZnO acted as an electrical emitter layer on a p-type c-Si substrate for photovoltaic applications and obtained PCE of 17.16% for the ZnO:B(n)/ZnO/c-Si(p) solar cell,  $V_{oc} = 0.675$  V,  $I_{sc} = 0.302$  A and FF 83.96% via the simulation approach.<sup>25</sup> Pietruszka et al. prepared ZnO/Si HJ-based solar cells using atomic layer deposited ZnO on p-type Si and demonstrated the PCE of 14%.<sup>26</sup> It is reported from our group that Shah et al. performed a simulation study to investigate the optoelectrical properties of the Ag-ZnO/ZnO double ARC layer-based c-Si solar and possessed the PCE of 14.82% when the carrier lifetime of 10  $\mu$ s and carrier concentration of  $1 \times 10^{17}$   $cm^{-3}$ .<sup>27</sup>

In the present paper, a simulation was carried out using the PC1D program to study a simple heterojunction solar cell based on n-type ZnO and p-type Si.<sup>28–30</sup> The optoelectrical properties were studied by varying parameters like thickness and doping concentration of the base and emitter to obtain the best conversion efficiency of solar cell.<sup>31–33</sup> In this simulation study, the deposition of a single ZnO layer on the Si substrate to form the single HJ which significantly reduces the average reflectance of the Si wafer by 7.65% in the wavelength range of 400–1000 nm. The ZnO/Si HJ-based c-Si solar exhibits a reasonably high efficiency ( $\eta = 24.8\%$ ) at a 400  $\mu$ m base thickness, 20  $\mu$ m emitter thickness, doping concentration of  $1.1 \times 10^{17}$   $cm^{-3}$  in the base and a doping concentration of  $5.1 \times 10^{16}$   $cm^{-3}$  in the emitter.

## Device Structure and Modeling Parameters

Most of the solar spectrum is absorbed in the front of the solar cell, so n-type silicon is placed at the front due to better surface quality than the p-type. So, the backside of the cell is the positive terminal, and the top of the cell is negative. The back contact does not necessary have to be transparent because it is far from the junction, so, it is not important in comparison to the front surface. Nowadays, the optimization of thickness of the back contact is carried out to increase the overall efficiency of the cells.<sup>34</sup> The layers in this solar cell also are ordered according to bandgap energy, with the layer with the lowest bandgap on the bottom and the layer with the highest bandgap on the top surface.<sup>35,36</sup> The reason for this is that a layer with a high bandgap can absorb the shorter wavelengths of the solar spectrum. The impact of doping concentration and thickness of the photovoltaic properties of the n-ZnO/p-Si solar cell was induced by the PC1D simulation tool.<sup>37,38</sup>

Personal computer one-dimensional (PC1D) principles are introduced in this section and are the foundation for simulation calculations. PC1D is a finite-element program for modeling semiconductor devices that uses finite elements.<sup>39–41</sup> A n-ZnO/p-Si single HJ-based solar cell is designed in PC1Dmod Ver.6.2. with a 1  $cm^2$  cross-sectional area, with series and shunt resistance. The schematic diagram for the solar cell modeled in PC1D is presented in Fig. 1. The simulation is run with a single sun intensity (0.1 W/ $cm^2$ ) and an air mass of AM1.5. The carrier's excitation is divided into 16-time steps, with the ambient temperature set at 25°C. The inset numerical value of parameters of the n-ZnO/p-Si HJ is listed in Table I. A p-type Si was employed as the absorber layer and n-type ZnO was used as the window layer in this proposed model.

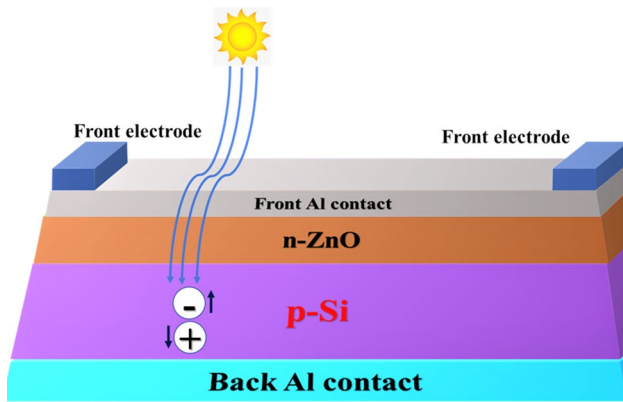


Fig. 1 Schematic diagram of n-ZnO/p-Si single HJ-based solar cell.

Table I Parameters used in the PC1D simulation tool

Parameters	ZnO	Si
Electron/Hole mobility ( $\text{cm}^2/\text{Vs}$ )	50	1500
Dielectric constant	8.66	11.9 [32]
Bandgap (eV)	3.27 [37]	1.124 [41]
Refractive index	2	3.44 [15]
n-Type background doping ( $\text{cm}^{-3}$ )	$2.2 \times 10^{19}$	–
p-Type background doping ( $\text{cm}^{-3}$ )	–	$1 \times 10^{16}$
Peak rear p-type doping ( $\text{cm}^{-3}$ )	–	$3 \times 10^{18}$
Bulk electron/hole recombination time ( $\mu\text{s}$ )	$1 \times 10^{-6}$	100
Electron/hole front surface recombination velocity ( $\text{cm/s}$ )	$1 \times 10^7$	$1 \times 10^6$ [38]

## Results and Discussion

### Influence of Thickness of Base and Emitter on Optical Properties

The incident light is trapped into the cell by texturing the front surface to enhance the photocurrent. The texturization of the front surface allows the confinement of solar radiation in the solar material by creating pyramids which are generally formed by etching the surface with acid ( $\text{H}_2\text{SO}_4$ ,  $\text{HNO}_3$ , etc.) or with alkaline etching ( $\text{NaOH}$ ,  $\text{KOH}$ , etc.).<sup>42</sup> This layer has an optimal angle to trap the light to optimize absorption. The role of texturization is very important; it is used to minimize losses by reflection.<sup>43</sup> Retaining a HJ at the rear surface and passivating it with silicon oxide and hydrogen considerably reduces the concentration of surface recombination states, resulting in reducing the surface carrier recombination.<sup>44</sup> The top surface texturing helps to decrease surface resistance and increase the probability of photon absorption.<sup>45</sup> The average reflectances for textured Silicon and ZnO/Si

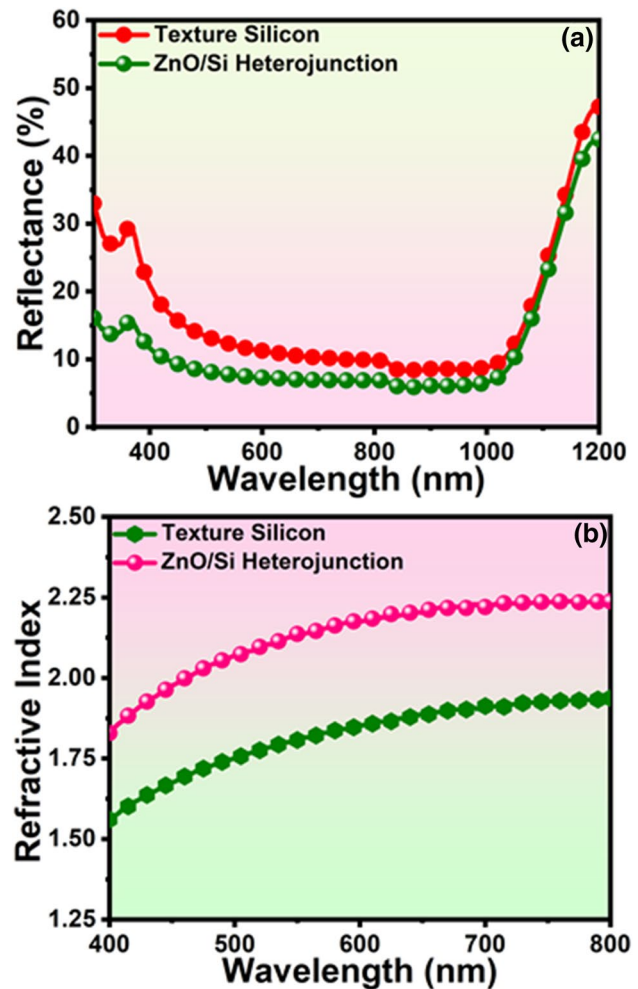


Fig. 2 (a) Reflectance spectra and (b) refractive index of textured Silicon and ZnO/Si HJ-based c-Si solar cells.

HJ-based silicon are recorded as 12.17%, and 7.65% in the wavelength range of 400–1000 nm, respectively, as shown in Fig. 2a. As compared to  $\text{SiN}_x$  ARC, ZnO/Si HJ-based silicon layers have exhibited a low average reflectance. From the reflectance measurement, the refractive index of the HJ is calculated.<sup>46</sup> The numerical value of the refractive index between 2.0–2.3 is considered better for surface passivation in comparison to any refractive indices with ARC materials.<sup>47</sup> A refractive index of  $\sim 2.1$  is obtained for ZnO/Si HJ-based silicon, which is higher than other textured silicon which is tabulated in Table II, determined from Fig. 2b. This observed average refractive index is similar to the refractive indices of  $\text{SiO}_2$ ,  $\text{SiO}_2\text{-TiO}_2$ , and other oxide ARC materials.<sup>48</sup>

### Influence of Base Parameters on Cell Performance

It has been found that even small changes in the thickness of the base of the solar cells result in noticeable variation of

**Table II** Optoelectrical parameters of the HJ-based c-Si solar cells

Samples	Reflectance (%)	Refractive Index	$I_{sc}$ (A)	$V_{oc}$ (V)	$I_{mp}$ (A)	$V_{mp}$ (V)	$P_{max}$ (W)	FF (%)	Efficiency (%)
Textured silicon	12.17	1.79	0.287	0.643	0.152	0.610	0.152	70.02	13.27
ZnO/Si HJ	7.65	2.10	0.403	0.729	0.232	0.681	0.232	75.25	24.8

$I_{sc}$  and  $V_{oc}$  and that affects the overall performance of c-Si solar cells.<sup>49</sup> The base region with a higher doping density level possesses the high  $V_{oc}$  and lowers the resistance, but it may also damage the lattice crystal.<sup>50</sup> It is known that the base region is a weakly doped (fewer barriers) region in the SHJ when compared to the other regions. The heterojunction formation between the oxide and c-Si absorption layer generally overcomes the barriers at the front and back interfaces for higher carrier transport.<sup>51</sup> Moreover, by the light soaking, the barriers over the SJH solar cell are more reduced by the healing of structural defects and unwanted lattices.<sup>51</sup> The thickness of the base region is optimized by adjusting thickness and doping levels by introducing simulation parameters by PC1D software. The optimization of  $I_{sc}$ ,  $V_{oc}$ ,  $P_{max}$ , and PCE have been investigated by varying the thickness of the base region from 60  $\mu\text{m}$  to 600  $\mu\text{m}$  and doping concentration from  $1.1 \times 10^{16} \text{ cm}^{-3}$  to  $1.1 \times 10^{18} \text{ cm}^{-3}$ . The maximum  $I_{sc} = 0.396 \text{ A}$  is recorded at a 400  $\mu\text{m}$  base thickness & a doping concentration of  $1.1 \times 10^{17} \text{ cm}^{-3}$  and maximum  $V_{oc} = 0.743 \text{ V}$  at a 100  $\mu\text{m}$  base thickness at the same doping concentration as shown in Fig. 3a, b. Similarly, the maximum power  $P_{max} = 0.241 \text{ W}$ , and maximum efficiency  $\eta = 24.2\%$  are achieved at a 400  $\mu\text{m}$  base thickness & doping concentration of  $1.1 \times 10^{17} \text{ cm}^{-3}$  as shown in Fig. 4a, b.

### Influence of the Emitter Parameters on the Cell Performance

A large portion of the radiation is absorbed by the top surface by thinning the top layer, a large fraction of the charge carriers produced by the incoming light is created within a diffusion length of the *p-n* junction.<sup>52</sup> The conductivity increases with an increase in the doping level of the region. So, an emitter with a high doping density is suitable for contact with a transparent conducting oxide (TCO); however, it has drawbacks like the reduction of  $I_{sc}$  through optical absorption.<sup>53</sup> The conductivity of the emitter region is lowered if the doping level is reduced, resulting in a decrease in  $V_{oc}$  and FF.<sup>54</sup> The front region of the junction is doped sufficiently to conduct the generated electricity without resistive losses. Excess doping density can degrade the quality of the material to the point where carriers recombine before reaching the junction. The thick and moderately doped passivated emitter regions have a low influence on the total recombination density.<sup>55</sup> Herein, a method has been proposed for evaluating the optimum

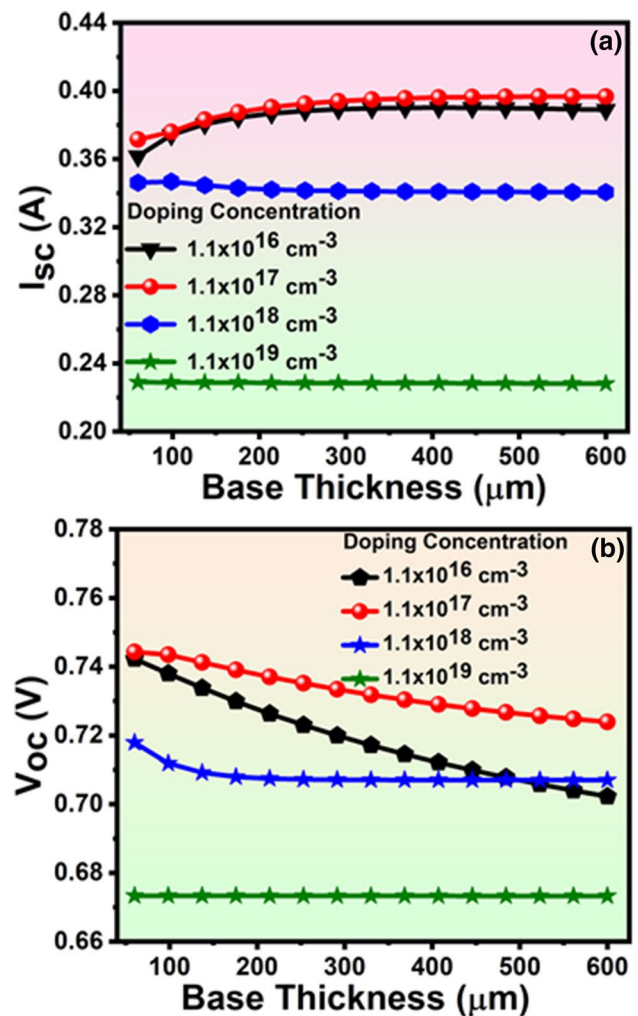


**Fig. 3** Variation in (a)  $I_{sc}$  and (b)  $V_{oc}$  with respect to doping concentration and a base thickness of ZnO/Si HJ-based c-Si solar cell.

thickness of a monofacial solar cell that was subjected to irradiation with charged particles.<sup>56</sup> The optimization of  $I_{sc}$ ,  $V_{oc}$ ,  $P_{max}$ , and PCE have been checked by varying the thickness of the emitter region from 0 to 50  $\mu\text{m}$  and doping concentration from  $5.1 \times 10^{16} \text{ cm}^{-3}$  to  $5.1 \times 10^{18} \text{ cm}^{-3}$ . The short-circuit current ( $I_{sc}$ ) gradually decreases with the increasing thickness of the emitter due to the large decrease in the number of short-wavelength photons available in the space charge region. The photovoltaic efficiency has the same shape as the open-circuit voltage; it

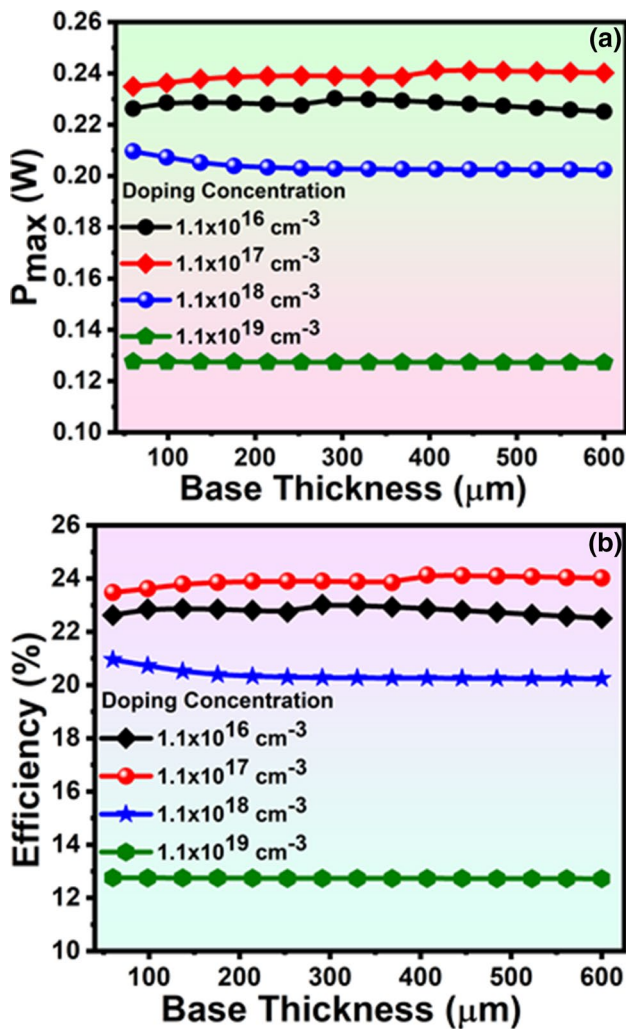


Fig. 4 Variation in (a)  $P_{max}$  and (b) efficiency with respect to doping concentration and a base thickness of ZnO/Si HJ-based c-Si solar cell.

decreases rapidly in the positive direction of the emitter thickness. The  $I_{sc}$  and  $V_{oc}$  of higher doping levels in the emitter are more sensitive than those of a lower doping level emitter when its thickness increases. The emitter collection efficiency decreases significantly due to band-gap narrowing and auger recombination effects.<sup>55</sup> The maximum  $I_{sc} = 0.4 \text{ A}$  is recorded at a  $20 \mu\text{m}$  emitter thickness & doping concentration of  $5.1 \times 10^{16} \text{ cm}^{-3}$  and maximum  $V_{oc} = 0.73 \text{ V}$  at a  $20 \mu\text{m}$  base thickness at the same doping concentration, as shown in Fig. 5a, b. Similarly, The maximum power ( $P_{max}$ ) =  $0.245 \text{ W}$ , and maximum efficiency ( $\eta$ ) =  $24.57\%$  are achieved at a  $20 \mu\text{m}$  base thickness & doping concentration of  $5.1 \times 10^{16} \text{ cm}^{-3}$  as shown in Fig. 6a, b.

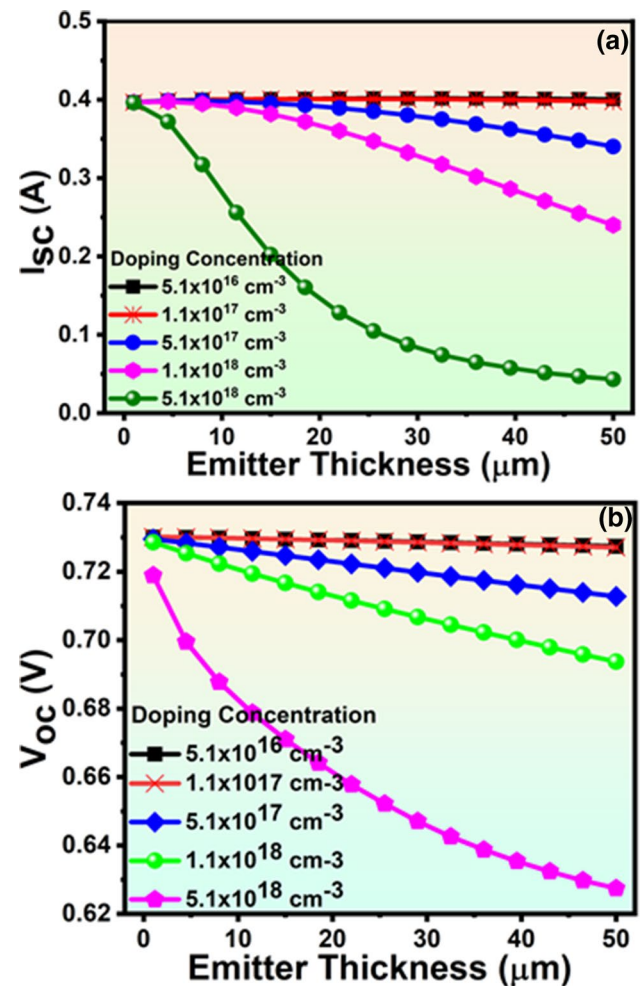


Fig. 5 Variation in (a)  $I_{sc}$  and (b)  $V_{oc}$  with respect to doping concentration and emitter thickness of ZnO/Si HJ-based c-Si solar cell.

### Photovoltaic Properties of Solar Cell

The supreme parameters are the current, voltage, and power to explain the overall efficiency of the solar cell. Quantum efficiency (QE) is also one of the most important characteristics to estimate the performance and  $I_{sc}$  of the solar cell in a particular wavelength range. By considering the optical properties of ZnO/Si HJ-based c-Si solar cell, the modeling capabilities of the PC1D simulation tool were used to investigate photovoltaic properties including  $I$ ,  $P$ - $V$ , and QE. The value of photocurrent ( $I_L$ ) generated by solar cells exposed under solar radiation is determined by the following equation:<sup>11</sup>

$$I_L = Q \int_0^\infty N(E)QE(E)(1 - R(E))dE \quad (1)$$

where  $N(E)$  = incident photon flux density,  $QE(E)$  = internal quantum efficiency and  $R(E)$  = reflectance. Generally, the semiconductor materials cannot absorb photons having low

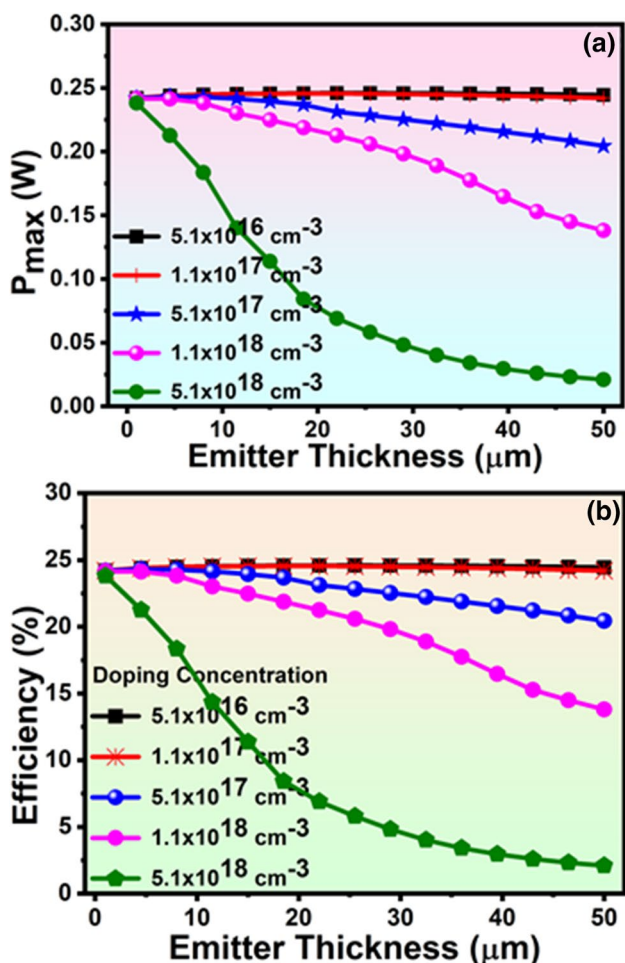


Fig. 6 Variation in (a) Pmax and (b) efficiency with respect to doping concentration and emitter thickness of ZnO/Si HJ-based c-Si solar cell.

energy. An ideal solar cell is thought of as a constant-current source connected to a diode that simulates photogenerated charge carrier recombination.

The simulation results exhibited the highest values of  $I_{sc} = 0.40$  A,  $V_{oc} = 0.729$  V,  $I_{mp} = 0.232$  A,  $V_{mp} = 0.681$  V,  $P_{max} = 0.232$  W for the HJ-based c-Si solar cell as shown in Fig. 7a. The simulated photovoltaic properties for textured silicon are tabulated in Table II. The internal quantum efficiency (IQE) and external quantum efficiency (EQE) of c-Si solar cells based on ZnO/Si HJ demonstrated the over 95% and 80% absorption covering respectively in the range of wavelength 300-1200 nm as shown in Fig. 7b. Blue photon absorption is more likely to occur near the top of the HJ, where all charge carriers are meant to travel to the p-n junction. Through the study of different parameters, we were able to optimize the physical and geometric parameters of a c-Si solar cell as shown in Table III, resulting in improved overall performance. Moreover, the comparative study of PV parameters of

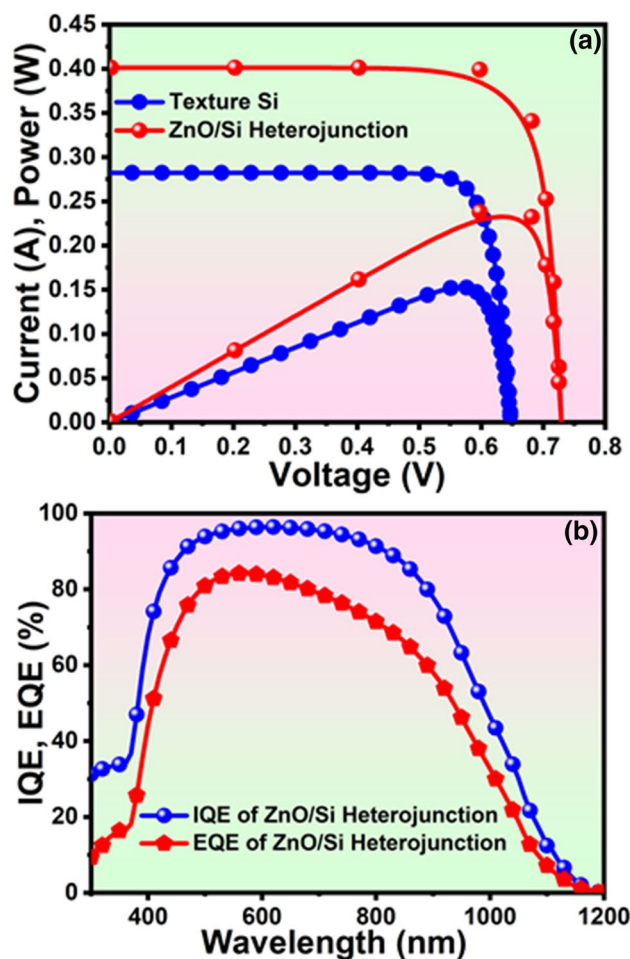


Fig. 7 Evaluation of (a) I, P-V, and (b) quantum efficiency of ZnO/Si HJ-based c-Si solar cell.

Table III Optimized value of parameters for proposed ZnO/Si HJ based c-Si solar cell

Parameters	Optimized value
Base thickness	400 μm
A doping concentration of the base	$1.1 \times 10^{17} \text{ cm}^{-3}$
Emitter thickness	20 μm
A doping concentration of the emitter	$5.1 \times 10^{16} \text{ cm}^{-3}$

reported HJ-based c-Si solar cells has been summarized in Table IV.

### Conclusion

In summary, the complete n-ZnO/p-Si HJ-based c-Si solar cells have been optimized as functions of surface recombination rate, base layer, emitter thickness, and surface doping level in a highly doped n-type area. The optimization of

**Table IV** Comparative study of reported ZnO/Si HJ based c-Si solar cell

Types of HJ Solar cell	$I_{sc}$ (A)	$V_{oc}$ (V)	FF (%)	Efficiency (%)	References
ZnO/Si	0.282	0.360	86.19	5.91	57
Al-ZnO/MIG-Si	0.185	0.670	85.15	10.35	57
ZnO/Si	0.380	0.520	71.00	14.0	26
ZnO/Si	0.377	0.662	81.50	20.34	58
HJ of Si	0.398	0.658	83.00	21.78	23
ZnO/Si	0.403	0.729	75.25	24.80	This work

thicknesses of the base and emitter with doping concentration has been carried out successfully by PC1D simulation software. The highest efficiency of 24.8% has been achieved at optimized thicknesses of the base and emitter layer. From the simulation, 400  $\mu\text{m}$  for the base thickness, 20  $\mu\text{m}$  for the emitter thickness, a base dopant density of  $1.1 \times 10^{17} \text{ cm}^{-3}$  and emitter dopant density of  $5.1 \times 10^{16} \text{ cm}^{-3}$  are the optimal values for n-ZnO/p-Si HJ-based c-Si solar cells. Therefore, this simulation study for the optimization of ZnO/Si-based c-Si solar cell would be one of the best possible upgrade alternative to the conventional single homo-junction c-Si solar cell.

**Acknowledgments** This work was supported by research funds from the Korea Institute of Energy Technology Evaluation and Planning (KETEP), Republic of Korea (Project No.: 20183010014270). This paper was supported by research funds from Jeonbuk National University in 2021. M. R. Siddiqui is grateful to the Researchers Supporting Project No. RSP-2021/326, King Saud University, Riyadh, Saudi Arabia.

**Conflict of interest** The authors declare that there is no conflict of interest regarding the publication of this paper.

## References

1. T. Koida, High-mobility transparent conductive oxide layers, *Spectroscopic Ellipsometry for Photovoltaics*. (Cham: Springer, 2018), pp. 565–586.
2. Y.-H. Son, P.T.M. Bui, H.-R. Lee, M.S. Akhtar, D.K. Shah, and O.-B. Yang, *Coatings* **9**, 631 (2019).
3. I.-S. Jung, J. Choi, D.K. Shah, and M.S. Akhtar, *J. Nanoelectron. Optoelectron.* **15**, 673 (2020).
4. X. Qing, C. Zhang, J. Gong, and S. Chen, *Vacuum*, **91**, 110391 (2021).
5. F. Mei, R. Li, and T. Yuan, *Tin Oxide Materials* (New York: Elsevier, 2020), pp. 579–597.
6. D.K. Shah, D. KC, M.S. Akhtar, C.Y. Kim, and O.-B. Yang, *Appl. Sci.* **10**, 6062 (2020).
7. D.K. Shah, Y.-H. Son, H.-R. Lee, M.S. Akhtar, C.Y. Kim, O.-B. Yang, *Chemical Physics Letters*, **754**, 137756 (2020).
8. S. Roguai, and A. Djelloul, *Appl. Phys. A Mater. Sci. Process.* **126**, 1 (2020).
9. D.K. Shah, S.Y. Han, M.S. Akhtar, O.-B. Yang, and C.Y. Kim, *J. Nanosci. Nanotechnol. Lett.*, **11**(2), 159 (2019).
10. V.A. Coleman, and C. Jagadish, *Zinc Oxide Bulk, Thin Films and Nanostructures* (New York: Elsevier, 2006), pp. 1–20.
11. Y. Liu, Y. Li, Y. Wu, G. Yang, L. Mazzarella, P. P.Moya, et al. *Materials Science and Engineering: R: Reports*, **142**, 100579 (2020).
12. D. KC, D.K. Shah, A. Shrivastava, *Materials Today: Proceedings*, (2021).
13. B. Hussain, A. Ebong, and I. Ferguson, *Sol. Energy Mater. Sol. Cells* **139**, 95 (2015).
14. U. Sikder, and M. Asif, *Opt. Laser Technol.* **79**, 88 (2016).
15. B. Hussain, A. Ebong and I. Ferguson, 2015 *IEEE 42nd Photovoltaic Specialist Conference (PVSC)*, 1–4, (2015).
16. L. Gerling, S. Mahato, C. Voz, R. Alcubilla, and J. Puigdollers, *Appl. Sci.* **5**, 695–705 (2015).
17. M. Labeled, N. Sengouga, A. Meftah, A. Meftah, Y. S. Rim, *Opt. Mater. (Amst.)*, **120**, 111453 (2021).
18. M. Taguchi, A. Yano, S. Tohoda et al., *IEEE J. Photovolt.* **4**, 96 (2014).
19. T. Mishima, M. Taguchi, H. Sakata, and E. Maruyama, *Sol. Energy Mater. Sol. Cells* **95**, 18 (2011).
20. Y. Tsunomura, Y. Yoshimine, M. Taguchi et al., *Sol. Energy Mater. Sol. Cells* **93**, 670 (2009).
21. L. Korte, E. Conrad, H. Angermann, R. Stangl, and M. Schmidt, *Sol. Energy Mater. Sol. Cells* **93**, 905 (2009).
22. S. Tohoda, D. Fujishima, A. Yano et al., *J. Non-Cryst. Solids* **358**, 2219 (2012).
23. S.-Y. Lien, Y.-S. Cho, Y. Shao, C.-H. Hsu, C.-C. Tsou, W. Yan, P. Han, D.-S. Wu, *In. J. Photoenergy*, **2015**, 273615, (2015).
24. D. KC., D.K. Shah, R. Waggle, A. Shrivastava, *J. Adv. Res. Dyn. Control Syst.*, **12**, 07-Special Issue, (2020).
25. L. Chen, X. Chen, Y. Liu, Y. Zhao, X. Zhang, *J. Semicond.*, **38**(5), 054005 (2017).
26. R. Pietruszka, B.S. Witkowski, E. Zielony, K. Gwozdz, E. Placzek-Popko, and M. Godlewski, *Sol. Energy* **155**, 1282 (2017).
27. D.K. Shah, D. KC, T-G Kim, M.S. Akhtar, C.Y. Kim, O-B Yang, *Opt. Mater.*, **121**, 111500 (2021).
28. G.S. Thirunavukkarasu, M. Seyedmahmoudian, J. Chandran, A. Stojcevski, M. Subramanian, R. Marnadu, S. Alfaify, and M. Shkir, *Energies* **14**, 4986 (2021).
29. D. KC, D.K. Shah, A.M. Alanazi, M.S. Akhtar, C.Y. Kim, and O-B Yang, *J. Electr. Mat.* **50**, 2199 (2021).
30. D.K. Shah, J. Choi, D. KC, M.S. Akhtar, C.Y. Kim, and O-B Yang, *J. Mater. Sci.: Mater. Electron.*, **32**, 2784 (2021).
31. Z.Y. Alami, M. Salem, M. Gaidi, and J. El, *MATEC Web Conf.*, **191**, 00013 (2018).
32. J. El Khamkhami, M. Salem, and M. Gaidi, *Society for science and education, UK*, **5**, 4 (2017).
33. S. Boudour, I. Bouchama, M. Hadjab, and S. Laidoudi, *Opt. Mater. (Amst)* **98**, 8 (2019).
34. <https://www.pveducation.org/pvcdrom/design-of-silicon-cells/silicon-solar-cell-parameters>
35. D.K. Shah, D. KC, M. Muddassir, M.S. Akhtar, C.Y. Kim, and O-B Yang, *Solar Energy*, **216**, 259 (2021).
36. D. KC, D.K. Shah, M.S. Akhtar, M. Park, C.Y. Kim, O.-B. Yang, and B. Pant, *Molecules* **26**, 3275 (2021).

37. K. Dasgupta, A. Mondal, S. Ray, and U. Gangopadhyay, *Silicon*, 2021.
38. M. Labed, N. Sengouga, A. Meftah, A. Meftah, and Y. S. Rim, *Opt. Mater. (Amst)*, 120, **8**, 111453 (2021).
39. X. Cai, X. Zhou, Z. Liu, F. Jiang, and Q. Yu, *Optik (Stuttg)* 164, 105 (2018).
40. L.A. Vilbois, A. Cheknane, A. Bensaoula, C. Boney, and T. Benouaz, *Energy Procedia* 18, 795 (2012).
41. A. Yadav, H. Yadav, V.K. Vashishtha, and M.K. Shivhare, Comparative performance evaluation of Si and Ge solar cell using PC1D modelling, *Recent Advances in Mechanical Engineering*. (Singapore: Springer, 2021), pp. 199–205.
42. <https://www.pveducation.org/pvcdrom/design-of-silicon-cells/surface-texturing>
43. Z. Tang, W. Tress, and O. Inganäs, *Mater. Today* 17, 389 (2014).
44. R.S. Bonilla, B. Hoex, P. Hamer, and P.R. Wilshaw, *Physica Status Solidi (a)* 214, 1700293 (2017).
45. M.S. Kim, J.H. Lee, and M.K. Kwak, *Int. J. Precis. Eng. Manufac.* 21, 1389 (2020).
46. S. Djearamane, L.S. Wong, Y.M. Lim, and P.F. Lee, *Sains Malays.* 48, 69 (2019).
47. J.D. Moschner, J. Henze, J. Schmidt, and R. Hezel, *Prog. Photovolt. Res. Appl.* 12, 21 (2004).
48. M. Jerman, Z. Qiao, and D. Mergel, *Appl. Opt.* 44, 3006 (2005).
49. M. Wolf, and E.L. Ralph, *IEEE Trans. Electron. Devices* 12, 470 (1965).
50. E.Y. Kim, and J. Kim, *Adv. Mater. Sci. Eng.* 2013, 1 (2013).
51. M. Mikolášek, Silicon heterojunction solar cells the key role of heterointerfaces and their impact on the performance, *Nanostructured Solar Cells*. (USA: InTech, 2017), p. 69.
52. C. Battaglia, A. Cuevas, and S.D. Wolf, *Energy Environ. Sci.* 9, 1552 (2016).
53. M. Bivour, C. Reichel, M. Hermle, and S.W. Glunz, *Sol. Energy Mater. Sol. Cells* 106, 11 (2012).
54. S. Kim, H. Park, D. P. Pham, Y. Kim, S. Kim, E-C. Cho, Y. Cho, and J. Yi, *Optik*, **235**, 166580 (2021).
55. N. Stem, and M. Cid, *Mater. Res.* 4, 143 (2001).
56. M.L. Ba, N. Thiam, M. Thiame, Y.T., M.S. Diop, M. Ba, C.T. Sarr, M. Wade, and G. Sissoko, *J. Electromagn. Anal. Appl.* **11**, 10, (2019)
57. E. Kozarsky, J. Yun, C. Tong, X. Hao, J. Wang, W.A. Anderson, *38th IEEE Photovoltaic Specialists Conference* (2012)
58. B. Hussain, A. Aslam, T. Khan, M. Creighton, and B. Zohuri, *Electronics* 8, 238 (2019).

**Publisher's Note** Springer Nature remains neutral with regard to jurisdictional claims in published maps and institutional affiliations.